

Assessing the Feasibility of a Grid-Tied Smart Hybrid Power System through Optimal Sizing under Various Weather Conditions

Montaser Abdelsattar*[‡], Abdelgayed Mesalam*, Abdelrahman Fawzi*, Ibrahim Hamdan*

*Electrical Engineering Department, Faculty of Engineering, South Valley University, Qena, 83523, Egypt

(Montaser.A.Elsattar@eng.svu.edu.eg, abdgdy2012@hotmail.com, abdrahmanfawazy@eng.svu.edu.eg, Ibrahimhamdan86@eng.svu.edu.eg)

[‡] Corresponding Author; Montaser Abdelsattar, Qena, 83523, Egypt, Tel: +201003166006,

Montaser.A.Elsattar@eng.svu.edu.eg

Received: 16.09.2023 Accepted: 23.10.2023

Abstract- The integration of hybrid renewable power systems (HRPSs) offers a viable solution to ensure access to green, most reliable, and cost-effective energy sources, aligning with the objectives of sustainable development. An empirical case study is presented, involving a grid-tied HRPS for various climatic areas in Egypt, to assess the effectiveness of the hybrid system under various weather conditions. This work introduces two optimizers for determining the appropriate design of a grid-tied HRPS that incorporates photovoltaic (PV) modules, wind turbines (WTs), and battery banks (BBs). The major goal of this work is to implement smart strategies for managing the energy interchange between the HRPS and utility grid, to achieve design objectives. This research article provides a fair comparison of two optimizers, namely atom search optimization (ASO) and zebra optimization algorithm (ZOA), offering an in-depth evaluation of their performance and effectiveness. A mathematical model of the entire system is presented in this study, and it is simulated by MATLAB software. The simulation outcomes confirm the superior performance of the ZOA algorithm over the other optimizer, demonstrating its potential to deliver promising solutions. According to the results, installing the proposed hybrid system in the New Alamein region instead of the other site would save costs and reduce carbon emissions.

Keywords Grid-tied hybrid renewable power system, optimal design, multi objectives optimization, atom search optimization (ASO), zebra optimization algorithm (ZOA).

1. Introduction

Over the past few decades, the rise in global population and the expansion of industrial sectors have led to a notable upswing in electricity requirements. Presently, a substantial portion of electricity production heavily depends on finite fossil fuels like oil, natural gas, and coal. In actuality, these resources cater to more than 70% of the global energy demand [1], [2]. The substantial surge in energy requirements along with the negative ecological consequences linked to fossil fuels has prompted several countries to seek ways of fulfilling their energy needs through the utilization of green and more sustainable power sources. In the lead-up to the 26th Conference of the Parties (COP26), numerous nations have unveiled fresh commitments detailing their contributions to the global effort of attaining climate goals, particularly aiming for net zero emissions targets. In line with this trajectory, the

majority of newly added electricity generation capacity by 2030 will stem from low-emission sources, with wind turbines (WTs) and photovoltaic (PV) alone accounting for nearly 500 GW on an annual basis. Consequently, the utilization of coal in electricity generation is anticipated to decrease by 20% from its recent peak by 2030. If all the announced commitments are effectively put into action, global CO₂ emissions stemming from electricity production are projected to witness a 40% reduction by 2050 [3].

Combining wind and solar power generation can help overcome the limitations of each renewable energy source (RES) individually. WT's output fluctuates based on variable wind speeds. PV modules only produce power during daylight hours. However, integrating wind and solar together can minimize fluctuations and enable more consistent power production day and night. The complementary nature of wind and solar can lead to a more reliable HRPS [4]. Egypt receives

abundant sun (3100 hours of sunshine annually, translating to 9 to 11 hours daily across the country) and moderate winds (ranging from 5 to 10 m/s in some regions) ideal for renewable energy generation, yet currently relies mainly on fossil fuels for electricity. This heavy fossil fuel use results in over 223 million tons of CO₂ emissions annually, impacting the environment negatively. Working to change this, Egypt now has a national plan to significantly increase renewable energy production over the next decade, with wind and solar together potentially supplying around 40% of the country's electricity by 2035 (14% from WTs & 25% from PV) [5].

Hybrid renewable power systems (HRPSs), comprising hybrid electricity sources, can operate in independent or grid-tied modes. The grid-dependent mode facilitates trading with the utility grid, making the system a revenue source and incentivizing investments in the power sector. By allowing the HRPS to sell excess electricity to the grid, it becomes economically viable and attractive for stakeholders to participate and invest in the system. This trading option enhances the financial sustainability and attractiveness of HRPSs as a renewable energy solution [6]. Connection with the utility grid offers two options: purchasing power only during energy deficit periods or enabling power exchange with the utility grid (purchasing electricity & selling excess power). Net metering and feed-in tariffs (FIT) are used to account for electricity exchange. In net metering, bidirectional meters are employed to measure both energy consumption from the grid and surplus generation that is fed back into the grid. FIT calculates compensation for injected power into the utility grid [7].

Obtaining the perfect design of HRPS presents a significant challenge, with the major goal being to decrease the expenses of electricity production while ensuring uninterrupted power provision (robust reliability) and at lowest pollution emissions. Optimal sizing of HRPSs involves the utilization of different assessment criteria, encompassing economic indexes such as cost of energy (COE), reliability metrics such as loss of power supply probability (LPSP), and environmental considerations such as carbon emissions (CE) [8]. Various researchers have proposed a range of optimization algorithms aimed at tackling sizing challenges. Several examples of these approaches include: genetic algorithm [9], cuckoo search [10], simulated annealing [11], whale optimization algorithm (WOA) [12], grey wolf optimizer (GWO) [13], and improved multi-objective GWO [14].

In recent times, there has been a proliferation of studies that aim to elucidate and assess various aspects of grid-tied HRPSs. Minimizing the net present cost was the main objective for the perfect design of grid-tied HRPS comprising PV, a biomass generator (BG), and battery banks (BBs) [15]. In other research works, two objectives, namely COE and LPSP were considered to determine the optimal configuration of HRPS consisting of PV modules/WTs as well as a fuel cell and a utility grid as backup systems [16], [17]. Grid-dependent PV modules/WTs/BG hybrid system was optimized to decrease COE [18]. Four optimization algorithms were employed to determine the optimal sizing of HRPS connected to the grid incorporating PV modules, WTs, and pumped

hydro storage, with multiple objectives: optimizing the following, COE, fluctuations in the power supplied to the grid, LPSP, and complementary characteristics of renewable sources [19].

In Ref. [20], the optimal design of three HRPS configurations was evaluated using HOMER Pro (version 3.13.6): a grid-tied HRPS, a grid-tied HRPS with a FIT, and a standalone HRPS, all incorporating PV/WT/BB/diesel components. The outcomes indicated that the grid-tied HRPS with a FIT policy would result in the lowest NPC compared to the other configurations. HOMER software was utilized in Ref. [21] to optimize the COE in an HRPS comprising PV, BB, and diesel components. The outcomes showed that the COE was reduced to a value of 0.2386 \$/kWh. In Ref. [22], linear programming (linprog) in MATLAB was applied to optimize an HRPS comprising PV, WT, and BB components. The study revealed that the implementation of demand response resulted in a 65% reduction in BB size and a 28% decrease in the capital cost of the system.

The significant contributions of this study can be summarized as follows:

- Presenting a case study encompassing a grid-tied HRPS for two distinct climatic regions in Egypt, aiming to assess and quantify the system's operational efficiency across diverse weather conditions.
- Applying smart strategies to efficiently manage power interchange between HRPS and the electric grid, with the overarching goal of minimizing critical factors such as COE, LPSP, and CE as possible.
- Introducing a pair of optimizers to address the sizing dilemma and conducting an equitable comparative study to determine the superior option.

The paper's organization is outlined as follows: In Section 2, the mathematical modelling of the proposed grid-tied HRPS is elaborated, encompassing its components and strategy for power management. Section 3 delves into expense estimation, reliability, and CO₂ emissions assessment, while also introducing the optimization techniques utilized. The subsequent Section 4 is dedicated to presenting the results and discussions, highlighting outcomes for each location. The paper concludes in Section 5.

2. Modeling of Grid-Tied HRPS

In this section, the mathematical modeling of various components within the suggested grid-tied HRPS is detailed. This modeling is essential for the analysis of the system's overall performance. This grid-tied HRPS configuration incorporates several components, including PV modules, WTs, BBs, the electric grid, a bidirectional power converter, and a designated load, as illustrated in Fig. 1. The primary sources of energy in the system (solar & wind) are confronted with a significant challenge due to their intermittent nature. Consequently, BBs are utilized as primary backup systems to mitigate and address issues related to reliability. The electric grid acts as a secondary backup in situations where BBs are unable to meet the energy demand, and it also serves as a consumer of surplus energy once BBs are fully charged.

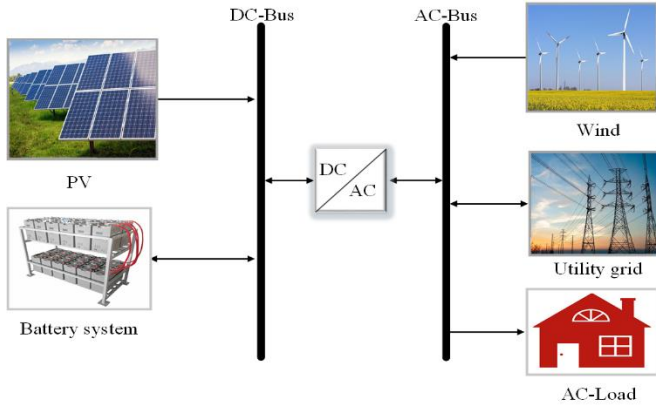


Fig. 1. Typical grid-dependent HRPS schematic.

2.1. PV Module

PV modules are a sustainable energy solution capable of capturing sunlight and transforming it directly into electric power. These PV modules are characterized by their simple installation process and minimal upkeep expenses. Their output power (P_{PVMs}) is primarily influenced by environmental factors such as solar radiation (R) and ambient temperatures (T_a) as follows [23], [24]:

$$P_{PVMs}(t) = N_{PVMs} * \eta_{PVMs} * P_{R_PVM} * \frac{R(t)}{R_N} [1 - \mu((T_a(t) + 0.034R(t)) - T_N)] \quad (1)$$

where, N_{PVMs} , η_{PVMs} , P_{R_PVM} , R_N , T_N , and μ are the total number, efficiencies, capacity, radiation under standard conditions, cell temperature at standard conditions, and temperature coefficient of PV modules, respectively.

2.2. Wind Turbine

The power generated by the WT is influenced by three primary factors: the wind speed at the chosen location, the height of the WT tower's hub, and the power output curve of the selected WT model. Converting the measured wind speed at an anemometer height to the relevant hub height is essential due to the variation of wind speed with altitude. The following formula can be employed to estimate wind speed at any desired height [25]:

$$\frac{V_{Hl}(t)}{V_l(t)} = \left(\frac{H_{Hl}}{H_l}\right)^{\beta_C} \quad (2)$$

where, $V_{Hl}(t)$, and $V_l(t)$ denote wind speed at a time t for required high H_{Hl} , and reference high H_l , respectively, β_C indicates friction coefficient. The actual power generated by WTs (denoted as $P_{WTS}(t)$) can be mathematically described as follows [26]:

$$P_{WTS}(t) = \begin{cases} N_{WTS} * \eta_{WTS} * P_{R_WT} * \frac{V^2(t) - V_L^2}{V_R^2 - V_L^2}, & V_L < V(t) < V_R \\ n_{WTS} * \eta_{WTS} * P_{R_WT}, & V_R < V(t) < V_H \\ 0, & V(t) < V_L \text{ or } V(t) > V_H \end{cases} \quad (3)$$

where, N_{WTS} , η_{WTS} , P_{R_WT} , V_R , V_L and V_H denote the total number, efficiencies, rated power, rated speed, lowest and highest wind speed limitations of WT, respectively.

2.3. Utility Grid

RESs, being inherently intermittent, require a secondary backup for sustained energy supply. In cases where the battery banks fail to meet the energy demand, the electrical grid steps in, providing the necessary power. The calculation for purchased power from the grid is governed by Eq. (4). Conversely, during surplus energy periods and following battery banks' full charge, excess energy is channeled back to the grid, with the computation outlined in Eq. (5) [27].

$$P_{GP}(t) = \min(P_{deficit}(t); P_{GP,Max}) \quad (4)$$

$$P_{GS}(t) = \min(P_{surplus}(t); P_{GS,Max}) \quad (5)$$

where, $P_{GP}(t)$ and $P_{GP,Max}$ indicate purchased power at a time t and maximum allowable purchased power from the grid, respectively, $P_{GS}(t)$ and $P_{GS,Max}$ signify sold power at a time t and maximum allowable sold power to the grid, respectively. While, $P_{deficit}(t)$ represents the energy deficit that occurs after the BBs discharge their stored energy completely, and $P_{surplus}(t)$ signifies the surplus energy that remains after the BBs have completed their charging process.

2.4. Battery Bank

The core function of battery bank is to store surplus energy generated by renewable sources, ensuring its availability for later use. During periods of higher power demand than renewable generation, the BBs can be discharged to meet the energy requirement, thereby acting as a primary backup for grid-tied HRPS, as articulated in Eq. (6). Conversely, in scenarios where renewable energy production exceeds energy for load demand, BBs are capable of recharging, as detailed in Eq. (7) [23], [28].

$$SOC(t) = SOC(t - 1)(1 - \beta_{BB}) - \left[\frac{P_L(t) - P_{WTS}(t)}{\eta_C} - P_{PVMs}(t) \right] \cdot \eta_{DB} \quad (6)$$

$$SOC(t) = SOC(t - 1)(1 - \beta_{BB}) + \left[\frac{P_{WTS}(t) - P_L(t)}{\eta_C} + P_{PVMs}(t) \right] \cdot \eta_{CB} \quad (7)$$

where, $SOC(t)$, $SOC(t - 1)$, β_{BB} , and $P_L(t)$ denote BB's state of charge at a time t , $t - 1$, self-discharge rate, and load demand, respectively, η_C , η_{CB} , and η_{DB} are converter, battery charging, and discharging efficiencies, respectively.

2.5. Bi-directional Converter

The illustrated hybrid system in Fig. 1 integrates both alternating current (AC) and direct current (DC) components, necessitating power electronics converters to facilitate bidirectional power conversion. These converters play a

crucial role in transforming AC power into DC and vice versa. The selection of the capacity for the bidirectional converter is driven by the maximum load demand (peak) as follows [29]:

$$P_{R_C} = \frac{P_{L_P}}{\eta_C} \quad (8)$$

where, P_{R_C} , η_C , and P_{L_P} denote rated power, efficiency of converter, and peak load demand, respectively.

2.6. Strategy for Power Management

The effective regulation of electricity generation to fulfill load demands is achieved through the implementation of a power management technique. This approach is depicted in the flowchart provided in Fig. 2. As per the flowchart sequence, surplus energy generated by sustainable resources is harnessed to recharge BBs. This occurs when renewable energy production exceeds load demands, resulting in a zero LPSP value. Any remaining surplus energy following full recharging is then fed into the grid. However, if sold power to the grid exceed the predefined limit ($P_{GS,Max}$), the surplus energy is redirected to a dumping load. In contrast, if the energy output from renewable sources falls short of the load demand, BBs enter a discharge mode to provide the necessary electricity. If the combined energy output from sustainable sources and BBs is still insufficient to meet the load demand, the electric grid intervenes to cover the energy gap. In scenarios where power is being procured from the grid, LPSP is set to zero if the purchased power from the grid is below a certain predefined limit ($P_{GP,Max}$). However, if the purchased

power exceeds this limit, the LPSP can be calculated using the formula that will be discussed in the following section.

3. Optimization Problem

3.1. Cost of Energy

COE is a prominent economic indicator frequently employed to evaluate the feasibility of hybrid systems. It can be computed based on the annual cost of the system (C_{Tot}^{Ann}) and the total load demand throughout the year. The COE calculation is expressed through Eqs. (9) and (10) [30]. The transition from the system's net present cost (NPC) to the annual total cost of the system is achieved through the application of the capital recovery factor (CRF^{i,m_P}), as determined by Eqs. (11), and (12) [31], [32].

$$COE = \frac{C_{Tot}^{Ann}}{\sum_{H=1}^{8760} PL} \quad (9)$$

$$C_{Tot}^{Ann} = C_C^{Ann} + C_{O\&M}^{Ann} + C_R^{Ann} + C_G^{Ann} \quad (10)$$

$$NPC = \frac{C_{Tot}^{Ann}}{CRF^{i,m_P}} \quad (11)$$

$$CRF^{i,m_P} = \frac{i(1+i)^{m_P}}{(1+i)^{m_P}-1} \quad (12)$$

In the above equations, C_C^{Ann} , $C_{O\&M}^{Ann}$, C_R^{Ann} , and C_G^{Ann} represent the yearly expenses associated with capital, maintenance, replacement, electricity exchange with the grid, respectively, m_P and i denote the project's lifespan and the interest rate, respectively.

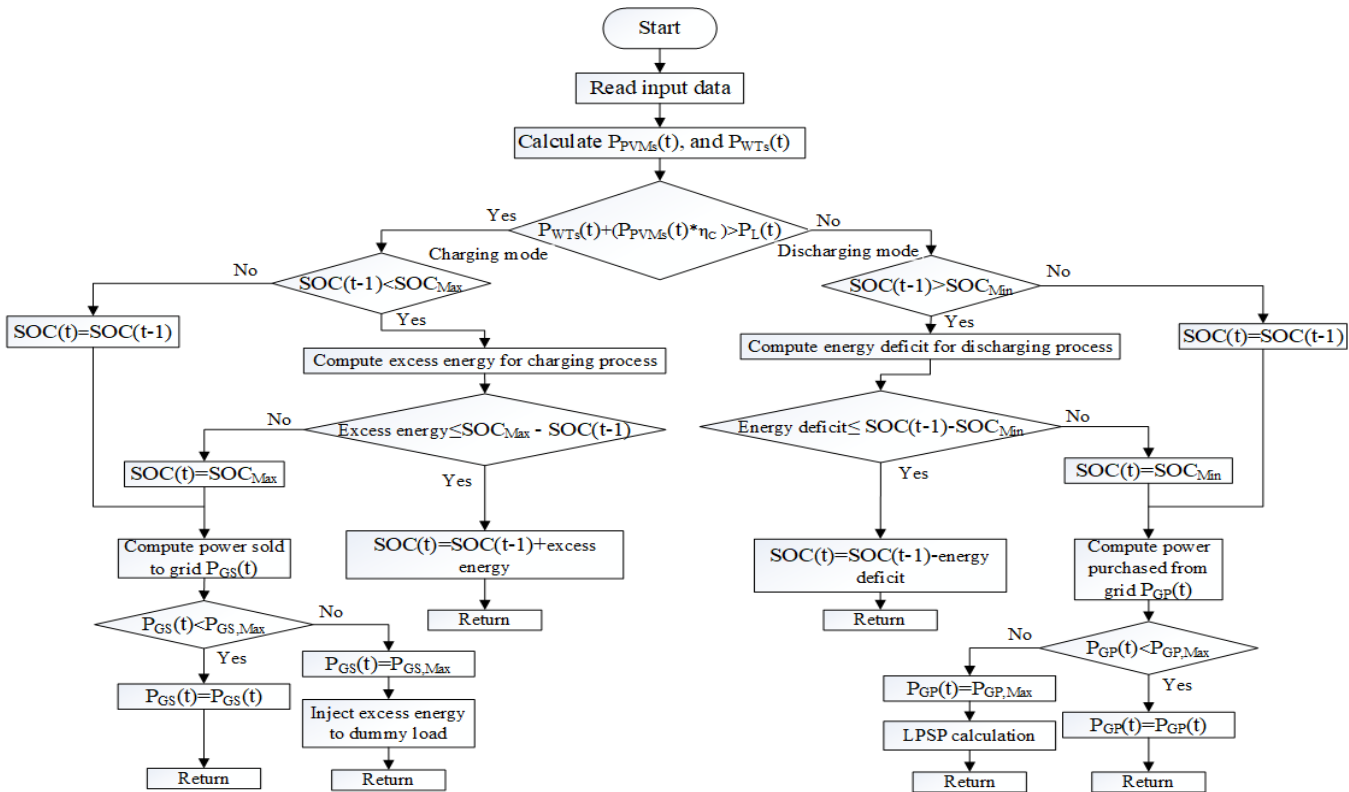


Fig. 2. Flowchart of strategies for power management.

3.1.1. The annual capital cost

The annual capital expenditures for all the equipment used in grid-tied HRPS can be calculated using the following formula [30], [33]:

$$C_C^{Ann} = 1.4 \cdot N_{PVMs} \cdot C_{C,PVM} \cdot CRF^{i,m_{PVM}} + 1.2 \cdot N_{WTs} \cdot C_{C,WT} \cdot CRF^{i,m_{WT}} + N_{Battery} \cdot C_{C,BB} \cdot CRF^{i,m_{BB}} + P_{R,C} \cdot C_{C,Conv} \cdot CRF^{i,m_{Conv}} \quad (13)$$

where, $C_{C,PVM}$, $C_{C,WT}$, $C_{C,BB}$, and $C_{C,Conv}$ represent the initial expenses of PV module, WT, BB, and converter, respectively. Additionally, m_{PVM} , m_{WT} , m_{BB} , and m_{Conv} indicate the lifespan of PV module, WT, BB, and converter, respectively. Regarding the PV part, the civil work and installation expenses have been accounted for as 40% of their initial cost. Similarly, for the WT's part, these expenses have been estimated at 20% of their initial cost [34].

3.1.2. Operating & maintenance cost

For calculating the yearly operational and maintenance expenditures of the hybrid system equipment, the following equation is applied:

$$C_{O\&M}^{Ann} = N_{PVMs} \cdot C_{O\&M,PVM} + N_{WTs} \cdot C_{O\&M,WT} + N_{Battery} \cdot C_{O\&M,BB} \quad (14)$$

where, $C_{O\&M,PVM}$, $C_{O\&M,WT}$, and $C_{O\&M,BB}$ denote yearly operational & maintenance expenses of PV module, WT, and BB, respectively. Maintenance expenses for the converter are not considered in this work.

3.1.3. The annual replacement cost

Throughout the project duration, some equipment within the hybrid system may need to be replaced multiple times. Except for the PV modules, which align with the project's lifespan, all other system components in this work require periodic replacement. The yearly replacement expenses for specific system components, as well as the aggregate replacement costs, can be calculated using the following formulas [35], [36]:

$$C_{R,WTs}^{Ann} = N_{WTs} \cdot C_{C,WT} \cdot \left(\frac{1}{(1+i)^{20}} \right) \cdot CRF^{i,m_{WT}} \quad (15)$$

$$C_{R,BBs}^{Ann} = N_{Battery} \cdot C_{C,BB} \cdot CRF^{i,m_{BB}} \cdot \sum_{m_{BB}=10,20} \frac{1}{(1+i)^{m_{BB}}} \quad (16)$$

$$C_{R,Conv}^{Ann} = P_{R,C} \cdot C_{C,Conv} \cdot CRF^{i,m_{Conv}} \cdot \sum_{m_{Conv}=10,20} \frac{1}{(1+i)^{m_{Conv}}} \quad (17)$$

$$C_R^{Ann} = C_{R,WTs}^{Ann} + C_{R,BBs}^{Ann} + C_{R,Conv}^{Ann} \quad (18)$$

In the above equations, $C_{R,WTs}^{Ann}$, $C_{R,BBs}^{Ann}$, and $C_{R,Conv}^{Ann}$ signify WT's, BB's, and converter yearly replacement costs, respectively. This research assumes a lifespan of 20 years for WT, 10 years for BB, and 10 years for the converter.

3.1.4. The annual cost of power exchange with the grid

The following equation is employed to assess the net cost associated with procuring electricity from the utility grid and selling surplus electricity back to the network [37].

$$C_G^{Ann} = C_P \sum_{t=1}^{8760} P_{GP}(t) - C_S \sum_{t=1}^{8760} P_{GS}(t) \quad (19)$$

where, C_P and C_S stand for the pricing associated with procuring electricity from the external grid and supplying electricity to the grid, respectively. According to the electricity tariff in Egypt, these prices are set at 0.08 \$/kWh and 0.2 \$/kWh, respectively.

3.2. Loss of Power Supply Probability

LPSP, a crucial design factor, quantifies the probability of the hybrid system's failure to satisfy load demands adequately. LPSP values are confined to a range of 0 to 1. The power deficit ($P_D(t)$) needs to be maintained at zero to guarantee a consistent supply of the total load. The LPSP value is determined using the following formula [38]:

$$LPSP = \frac{\sum_{t=1}^{8760} P_D(t)}{\sum_{t=1}^{8760} P_L(t)} \quad (20)$$

3.3. Pollution (CO₂) Emissions

This study is centred on addressing multiple objectives, one of which involves evaluating the environmental implications of a grid-tied HRPS. This assessment encompasses the crucial criterion of carbon emissions as an integral component of the sizing process. The emission of CO₂ from an electric grid (PE_{Grid}) is linked to the quantity of purchased power from the grid, a relationship that can be expressed as follows [39]:

$$PE_{Grid} = \sum_{t=1}^{8760} P_{GP}(t) * F_{E_Grid} \quad (21)$$

where, F_{E_Grid} represents the emission factor of the utility grid and is assigned a value of 0.632 kg/kWh [40].

3.4. Objective Function

The primary aim of sizing a grid-tied HRPS, as elucidated in this work, is to reduce the following criteria: $LPSP$, COE , and PE_{Grid} . These objectives are operationalized as follows:

$$OF = \min(\omega_1 \cdot LPSP + \omega_2 \cdot COE + \omega_3 \cdot PE_{Grid}) \quad (22)$$

In this study, weight values ω_1 , ω_2 , and ω_3 were meticulously selected to achieve a balance among different objectives and optimize the overall outcome of the multi-objective optimization process. Specifically, the weights chosen were 0.5999, 0.4, and 0.0001, respectively.

3.5. Constraints

To ensure proper functioning and prevent issues such as overcharging or undercharging, the components of grid-tied HRPS are subject to specific constraints. In this regard, BB's

have defined limits, as outlined in Eq. (23), which ensure that the maximum state of charge (SOC) (SOC_{Max}) corresponds to the full capacity of the BB, while the minimum SOC (SOC_{Min}) prevents the BB from being discharged excessively. Another imposed limitation in this study pertains to the upper limit of LPSP, which should not surpass 5%, as articulated in Eq. (24). Finally, constraints related to the power exchange with the grid are represented by Eqs. (25) and (26).

$$SOC_{Min} \leq SOC(t) \leq SOC_{Max} \quad (23)$$

$$LPSP \leq 5\% \quad (24)$$

$$P_{GP}(t) \leq P_{GP,Max} \quad (25)$$

$$P_{GS}(t) \leq P_{GS,Max} \quad (26)$$

3.6. Optimization Approaches

This study employs optimization algorithms; zebra optimization algorithm (ZOA) and atom search optimization (ASO) to address sizing challenges and achieve the optimal configuration of a grid-tied HRPS.

3.6.1. Zebra optimization algorithm

Introduced in 2022, the ZOA is a novel bio-inspired meta-heuristic algorithm that derives its core principles from the behavioural patterns of zebras in the wild [41]. This technique emulates the foraging patterns of zebras as well as their defensive methods against threats from potential predators. The following two stages illustrate two innate behaviours observed in zebras in the wild, which are employed to update the members of ZOA.

i. 1st stage; foraging behaviour

In the initial stage, the population members undergo updates that mimic the foraging behaviour of zebras in their quest for sustenance. The upgrade of zebras' position during this phase can be mathematically represented using the following equations.

$$y_{i,j}^{New,1} = y_{i,j} + R * (Z_j^P - E * y_{i,j}), \quad E \in \{1,2\} \quad (27)$$

$$Y_i = \begin{cases} Y_i^{New,1}, & OF_i^{New,1} < OF_i \\ Y_i, & else \end{cases} \quad (28)$$

In the above equations, $Y_i^{New,1}$, $y_{i,j}^{New,1}$, and $OF_i^{New,1}$ denote the updated condition of the i th zebra, its j th dimension value, and its corresponding objective function value as determined by the first stage, respectively, Z_j^P represents j th dimension of pioneer zebra, which signifies the best-performing member. Moreover, R indicates a number randomly chosen from the interval $[0, 1]$. Additionally, $E = Round(1 + Rand)$, where, $Rand$ denotes a randomly generated number within the range $[0, 1]$.

ii. 2nd stage; defence methods against predators

In the second stage, ZOA updates the positions of its population members in the search space by emulating the zebra's defensive methods against threats from potential predators. In this phase, it is assumed that either one of the following two defensive methods occurs with equal probability. Firstly, when zebras are exposed to lion attacks, they opt for an escape method that can be mathematically represented using mode S_1 in Eq. (29). Another scenario is when zebras face attacks from other predators, in which case they opt for an offensive strategy, modelled using the mode S_2 in Eq. (29). When upgrading the positions of zebras, if the newly generated position yields a superior value for the objective function, the zebra will adopt this new position. This updating rule is described by Eq. (30).

$$y_{i,j}^{New,2} = \begin{cases} S_1: y_{i,j} + K * (2R - 1) * \left(1 - \frac{t}{T}\right) * y_{i,j}, & P_s \leq \frac{1}{2} \\ S_2: y_{i,j} + R * (Z_j^A - E * y_{i,j}), & else \end{cases} \quad (29)$$

$$Y_i = \begin{cases} Y_i^{New,2}, & OF_i^{New,2} < OF_i \\ Y_i, & else \end{cases} \quad (30)$$

In the above equations, $Y_i^{New,2}$, $y_{i,j}^{New,2}$, and $OF_i^{New,2}$ denote the updated condition of the i th zebra, its j th dimension value, and its corresponding objective function value as determined by the last stage, respectively, t is a current iteration, while, T indicates maximum iterations. Moreover, K is a constant value that is set to 0.01, P_s signifies the probability employed to determine the selection of either of the two strategies, both of which are randomly generated within the range of $[0, 1]$. Additionally, Z_j^A represents the status of attacked zebra, and Z_j^A is its j th dimension value.

The ZOA algorithm's procedures and steps are illustrated in the flowchart provided in Fig. 3.

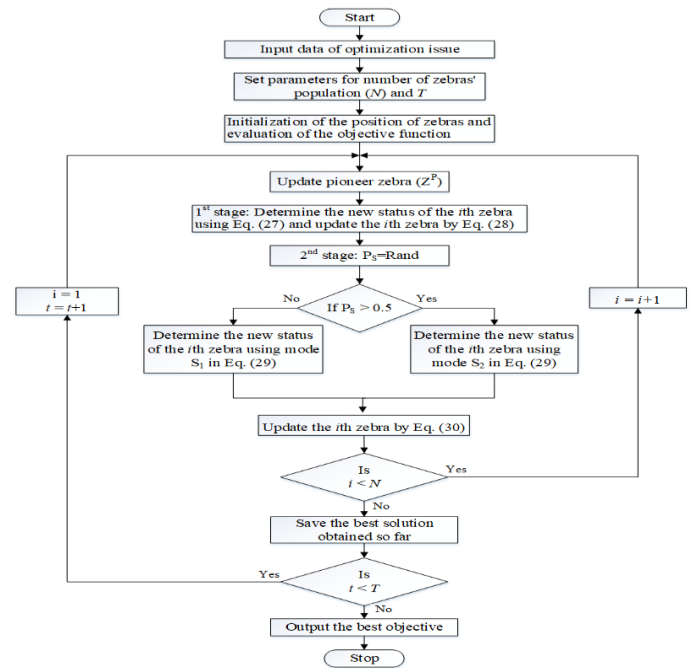


Fig. 3. Flowchart of strategies for power management.

3.6.2. Atom search optimization

Introduced in 2019, ASO is an optimization approach that draws inspiration from the molecular dynamics of atoms as described by atomic theory [42], [43]. In general, matter is composed of atoms that have mass and volume. These atoms interact with each other through microscopic interactions, regardless of the state of matter, and this interaction leads to complex structures. The interaction among atoms involves a pair of key characteristics: repulsive and attractive forces, as shown in Fig. 4. The repulsive force among atoms prevents overcrowding and trapping in local minima. When atoms move farther apart from each other, the repulsive force diminishes, intensifying the attractive force and guiding the search towards global minima. In ASO, atoms in the search space attract or repel each other based on their distance. Heavier atoms have slower acceleration, allowing them to exploit the local space more intensively. Conversely, lighter atoms have a high acceleration, enabling them to explore new regions in the search space. The iterative process persists until the solution convergence is achieved, which can be mathematically described by the following steps:

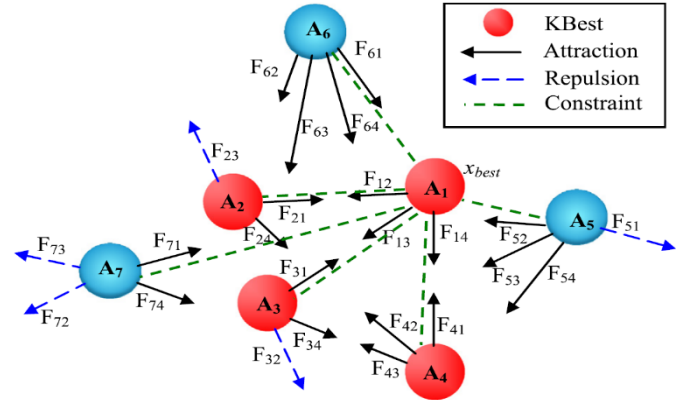


Fig. 4. Atomic forces system [42], [43].

The parameter K decreases over time to achieve this and can be considered as.

$$K = N - (N - 2) * \sqrt{\frac{t}{T}} \tag{36}$$

- i. **1st step:** Randomly initialize the decision variables and their positions are characterized as

$$X_i = (x_i^1, \dots, x_i^D), \quad i = 1, \dots, N \tag{31}$$

where, x_i^d ($d = 1, \dots, D$) denotes d^{th} position of i^{th} atom in D dimension space, N is atoms number.

- ii. **2nd step:** Commence by initializing atoms number, along with their positions, accelerations, mass, and velocity (v). Utilize the predefined parameters to determine the fitness function for each atom.
- iii. **3rd step:** Specify the mass of the atoms and the forces that operate among each atom as follows:

$$m_i(t) = \frac{E_i(t)}{\sum_{j=1}^N E_j(t)} \tag{32}$$

$$E_i(t) = e^{\frac{f_b(t) - f_i(t)}{f_w(t) - f_b(t)}} \tag{33}$$

where, $m_i(t)$ denotes i^{th} atom's mass at t^{th} iteration. Additionally, $f_b(t)$, $f_w(t)$, and $f_i(t)$ signify best, worst, and function of i^{th} atom fitness values at t^{th} iteration, respectively. $f_b(t)$, $f_w(t)$ are expressed as follows:

$$f_b(t) = \min_{i \in \{1, 2, \dots, N\}} f_i(t) \tag{34}$$

$$f_w(t) = \max_{i \in \{1, 2, \dots, N\}} f_i(t) \tag{35}$$

- iv. **4th step:** In the early iterations, atoms communicate with several neighbouring atoms to enhance exploration in the search space. Toward the later iterations, interactions with fewer K neighbours are focused on for better exploitation.

- v. **5th step:** Determine the interaction force ($F_i^d(t)$), and the constraint force ($G_i^d(t)$) at t^{th} iteration by Eqs. (37), and (38).

$$F_i^d(t) = \sum_{j \in K_{Best}} Rand_j F_{ij}^d(t) \tag{37}$$

$$G_i^d(t) = \beta e^{\frac{-20t}{T}} [x_b^d(t) - x_i^d(t)] \tag{38}$$

where, $Rand_j$ and β denote random values ranging among 0 and 1, and the multiplier weight, respectively. Moreover, $x_b^d(t)$ signifies d^{th} position of the optimal atom at t^{th} iteration.

- vi. **6th step:** Upgrade the acceleration, velocity, and position of each atom by the equations below.

$$A_i^d(t) = \frac{F_i^d(t)}{m_i^d(t)} + \frac{G_i^d(t)}{m_i^d(t)} = -\rho \left[1 - \frac{t-1}{T} \right]^3 e^{\frac{-20t}{T}} \sum_{j \in K_{Best}} \frac{Rand_j (2 \cdot (h_{ij}(t))^{13} - (h_{ij}(t))^7)}{m_i(t)} \tag{39}$$

$$\frac{[x_j^d(t) - x_i^d(t)]}{\|x_i(t), x_j(t)\|_2} + \beta e^{\frac{-20t}{T}} \frac{x_b^d(t) - x_i^d(t)}{m_i(t)}$$

$$v_i^d(t+1) = Rand_i^d v_i^d(t) + A_i^d(t) \tag{40}$$

$$x_i^d(t+1) = x_i^d(t) + v_i^d(t+1) \tag{41}$$

where, ρ and T represent depth weight and maximum iterations, respectively.

- vii. **7th step:** If the alteration in the fitness value is approaching the best-found value (x_b), acquire the optimized decision variables. Otherwise, iterate through Steps 2 to 7 until the termination condition is met. The ASO algorithm's summary is depicted in the flowchart presented in Fig. 5.

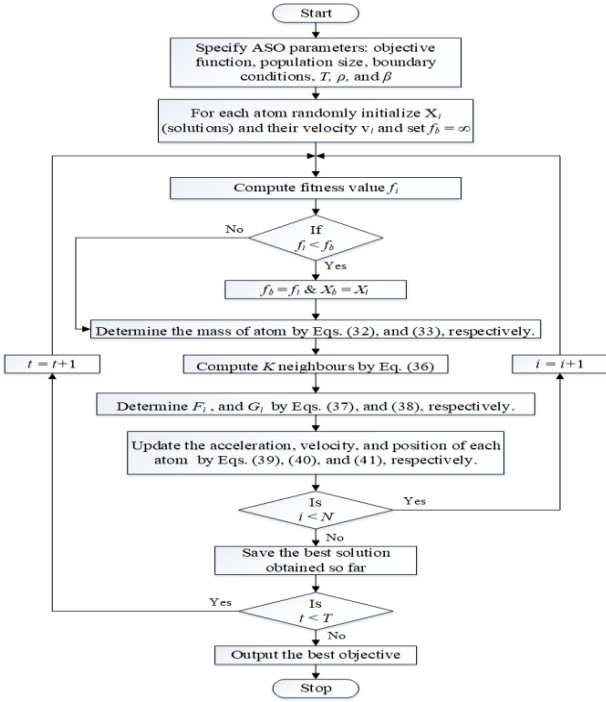


Fig. 5. Flowchart of ASO.

4. Simulation Results and Discussions

4.1. Study Region

This grid-dependent HRPS is studied across diverse weather conditions in two Egyptian towns: Ras Sudr and New Alamein. Ras Sudr is a town situated in the South Sinai Governorate of Egypt, positioned along the Gulf of Suez. On the other hand, New Alamein City is situated along the northern coastline and falls within the administrative boundaries of the Marsa Matrouh Governorate. Data for the study regions were collected across a one-year period, spanning 8760 hours. Figure 6 illustrates the mean monthly load demand during the same time frame. In Fig. 7(a) and (b), the monthly changes in radiation, ambient temperature, and wind speed are shown over a span of one year for Ras Sudr and New Alamein cities, respectively [44]. Several specifications of grid-dependent HRPS components are tabulated in Table 1 [45]. To ensure equitable comparison between both optimizers, the number of search agents and the maximum iterations for both were set at 20 and 50, respectively. Additionally, the parameters for each approach were kept consistent.

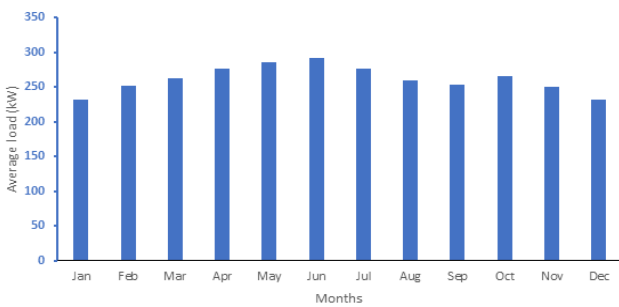
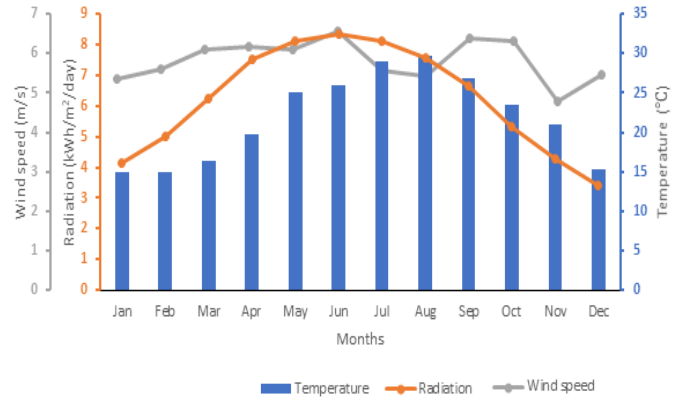
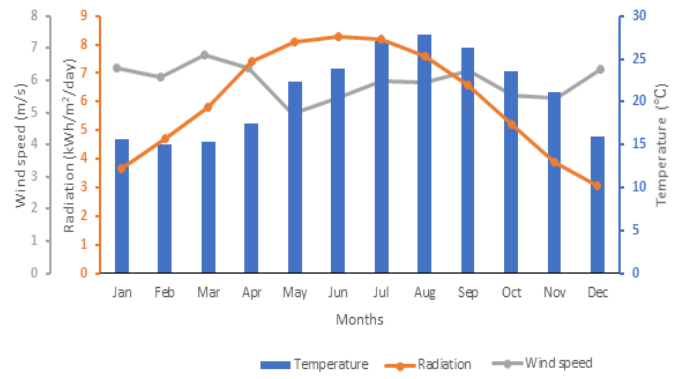


Fig. 6. The average monthly load demand.



(a)



(b)

Fig. 7. Weather data of a) Ras Sudr, and b) New Alamein city.

Table 1. Input parameters [45]

Components	Parameters	Values	Units
PV module	Model	PV – MLT260HC	
	$P_{R,PVM}$	260	W
	T_N	25	°C
	μ	0.004	1/°C
	R_N	1000	W/m ²
	$C_{C,PVM}$	112	\$/unit
	$C_{O\&M,PVM}$	1%	
	Lifespan	25	Years
WT	Model	Fuhrländer FL 30	
	$P_{R,WT}$	30	kW
	V_L	2.5	m/s
	V_H	25	m/s
	V_R	12	m/s
	$C_{C,WT}$	58564.79	\$/unit
	$C_{O\&M,WT}$	3%	
	Lifespan	20	Years
	Model	RS lead acid battery	
	Size	12V(50Ah)	
	β_{BB}	0.002	

Battery	η_{CB}	90%	\$/unit
	η_{DB}	85%	
	$C_{C, BB}$	146.5	
	$C_{O\&M, BB}$	3%	
	Lifespan	10	
Converter	η_C	95%	\$/kW
	$C_{C, Conv}$	711	
	Lifespan	10	
Others	m_P	25	Years
	i	6%	

4.2. An Optimum Design of the First Location

An in-depth study and comprehension of the available power sources at a given location are crucial for any project involving renewable energy. This understanding plays a pivotal role in accurate modelling and informed decision-making regarding the feasibility of the project. This subsection provides an overview of the results obtained from simulating the hybrid system at the initial site, "Ras Sudr". Following 50 iterations for ASO and ZOA, the ultimate outcomes and a comparison between both optimizers are summarized in Table 2. Illustrated in Fig. 8, ZOA exhibited more favourable results compared to the other optimizer. It attained the optimal solution of 0.084257 while staying within the predefined operational boundaries, achieving this outcome after just 13 iterations. Meanwhile, ASO attained the optimal solution of 0.0844 following undergoing 17 iterations. The most effective technique, ZOA, picked the optimal COE as 0.104073 \$/kWh, resulting in NPC of 3,048,356.4 \$ and an excellent LPSP of 2.4967×10^{-10} , aligning well with the appropriate value (<5%). Furthermore, ZOA predicted the lowest annual CO₂ emissions of 426,273.75 kg. ASO estimated COE of 0.10419 \$/kWh leading to NPC of 3,051,763.87 \$, LPSP of 1.2036×10^{-4} and annual CO₂ emissions of 426,515.94 kg. In accordance with the ZOA optimizer, for achieving the lowest COE, the recommended configuration entails 2000 PV modules, 20 WTs, and batteries count of 349.732 (equivalent to 350).

Furthermore, during times of energy deficit, a total of 674,483.79 kWh/year is procured from the grid. While, in instances of energy surplus, 604,163.12 kWh/year is sold back to the grid.

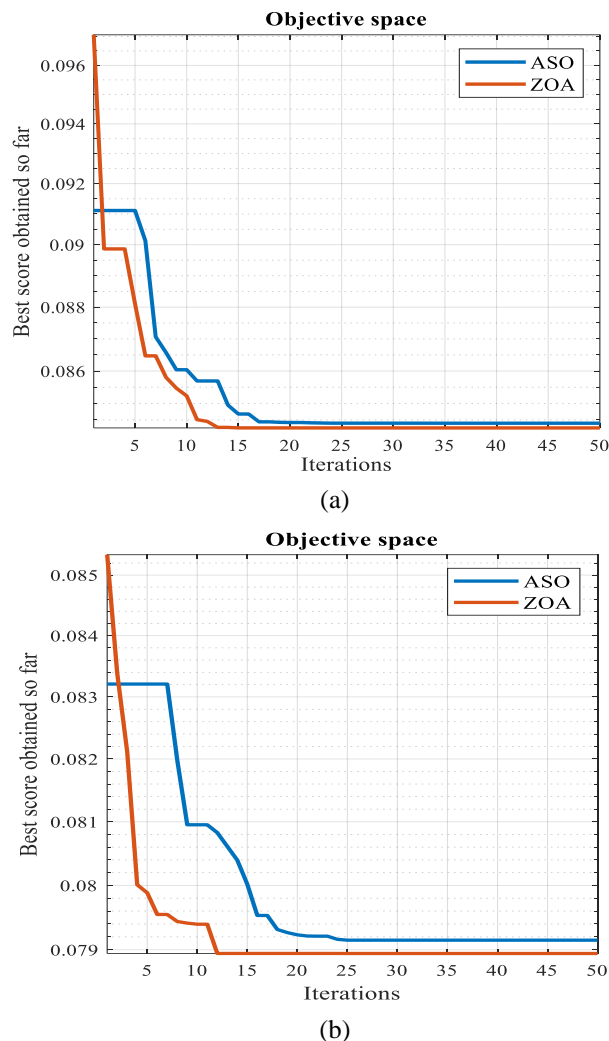


Fig. 8. The convergence curves of a) Ras Sudr, and b) New Alamein city.

Table 2. An overview of simulation results based on ASO and ZOA

Characteristics	Ras Sudr		New Alamein city	
	ASO	ZOA	ASO	ZOA
Best objective function	0.0844	0.084257	0.079149	0.078943
No. of iteration for the optimal solution	17	13	25	12
Number of PV	1998	2000	1995	2000
Number of WT	20	20	20	20
Number of batteries	351	350	445	444
purchased from grid (kWh/year)	674,866.99	674,483.79	642,331.39	640,831
sold to grid (kWh/year)	602,705.6	604,163.12	693,622.59	698,331.5
COE (\$/kWh)	0.10419	0.104073	0.096255	0.096106
NPC (\$)	3,051,763.87	3,048,356.4	2,819,346.98	2,814,983.28
LPSP	1.2036×10^{-4}	2.4967×10^{-10}	8.535×10^{-5}	1.5244×10^{-10}
Dummy Load (kwh/year)	2,117.2	2,124.3	3,013.9	3,067.5
Carbon emission (kg/year)	426,515.94	426,273.75	405,953.44	405,005.67

The ZOA technique's results are depicted in Fig. 9, including the hourly energy generation fluctuations for the components of the grid-dependent HRPS at this site. The simulation outcomes depicted in this figure demonstrate the energy contribution from PV modules (P_{PVMs}) and WTs (P_{WTs}), as well as the energy involved in charging & discharging the battery (E_{Ch} & E_{Dch}). Additionally, BB's SOC is depicted as a percentage of its total capacity (SOC %). Finally, it shows the energy exchange with the utility grid, highlighting the selling and buying of electricity throughout the operational timeframe (E_{GS} & E_{GP}).

Because of design limitations, meeting optimization criteria while entirely avoiding power exchange with the grid is extremely difficult. The figure demonstrates that electricity is consistently flowing to and from the utility grid. To provide a clearer insight into the strategy for power management underpinning the optimizers, the simulation outcomes are focused on a single day of the grid-tied HRPS's operation at its perfect conditions. Figure 10 depicts the simulation outcomes for a specific summer day (as an example, commencing at time 5064 and extending to 5088) concerning the optimal design determined by ZOA. At night and in the early morning, PV modules do not produce any electricity, and the power provided by WTs is insufficient to meet the demand. As a result, there is a positive power difference ($P_{Dif} = P_{Load} - (P_{PVMs} + P_{WTs})$), indicating that the power demand exceeds the combined power generated by PV modules and WTs. During these periods, BB discharges energy to fulfil the load requirements, and if the energy deficit remains, it is compensated by purchasing electricity from the grid. As the sun rises, the energy output from PV modules increases, leading BBs to commence charging from surplus energy until reaching their maximum permissible capacity (80%). As BBs charging completion, the excess power is consumed by the utility grid.

Based on the earlier showcased weather data, Ras Sudr experiences slightly higher radiation levels compared to New Alamein. Specifically, Ras Sudr has an annual average radiation of 6.23 kWh/m², whereas New Alamein records an average radiation of 6.04 kWh/m² annually. 77% of the overall energy for demand is provided by available sustainable sources (41% from WTs & 36% from PV), while, the remaining 23% is purchased from the electric grid as illustrated in Fig. 11(a). On the other side, 79% of the total energy consumption is provided to supply the load, while the remaining 21% is sold to a utility grid.

4.3. An Optimum Design of the Second Location

This subsection presents a summary of the simulation results conducted on the grid-tied HRPS at the second station, "New Alamein". The simulation outcomes demonstrate that, similar to the first location, ZOA yields superior results compared to ASO at this site as well. ZOA successfully reached the optimal solution of 0.078943 while adhering to the predetermined operational constraints, accomplishing this outcome after a mere 12 iterations. While, ASO achieved the optimal solution of 0.079149 after undergoing 25 iterations.

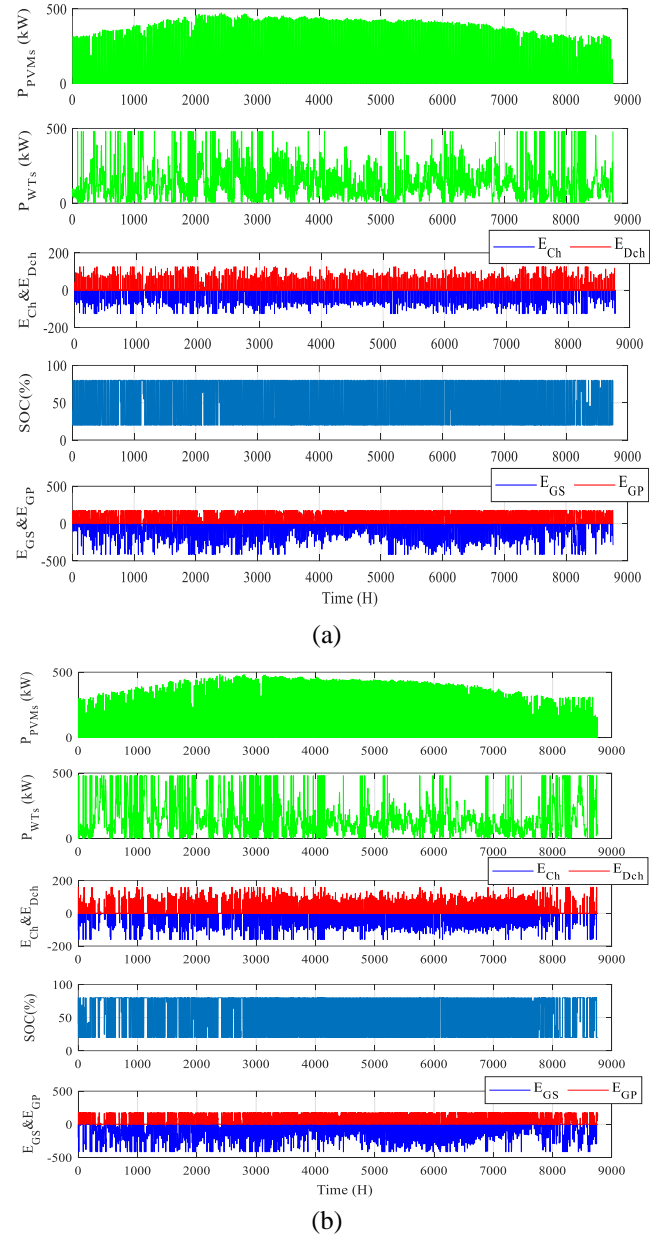


Fig. 9. ZOA technique results of an optimum design for 8760 h in a) Ras Sudr, and b) New Alamein city.

The most efficient approach, ZOA, identified the optimal COE as 0.096106 \$/kWh, leading to an NPC of 2,814,983.28 \$, which reflects a reduction of 7.7% compared to the scenario of installing this hybrid system at the first location, along with an excellent LPSP value of 1.5244×10^{-10} . Moreover, ZOA predicted the lowest annual CO₂ emissions of 405,005.67 kg, representing a 5% reduction compared to the emissions in the first site. According to the ZOA results, to achieve the lowest COE, the recommended configuration for this location involves 2000 PV modules, 20 WTs, and a battery count of 444.3595 (equivalent to 444). Additionally, during periods of energy deficit, a total of 640,831 kWh/year is procured from the grid, which represents a 5% reduction compared to that was purchased in the first site. Conversely, during times of energy surplus, 698,331.5 kWh/year is sold back to the grid, indicating an increase of 15.6% compared to that was sold in the first site.

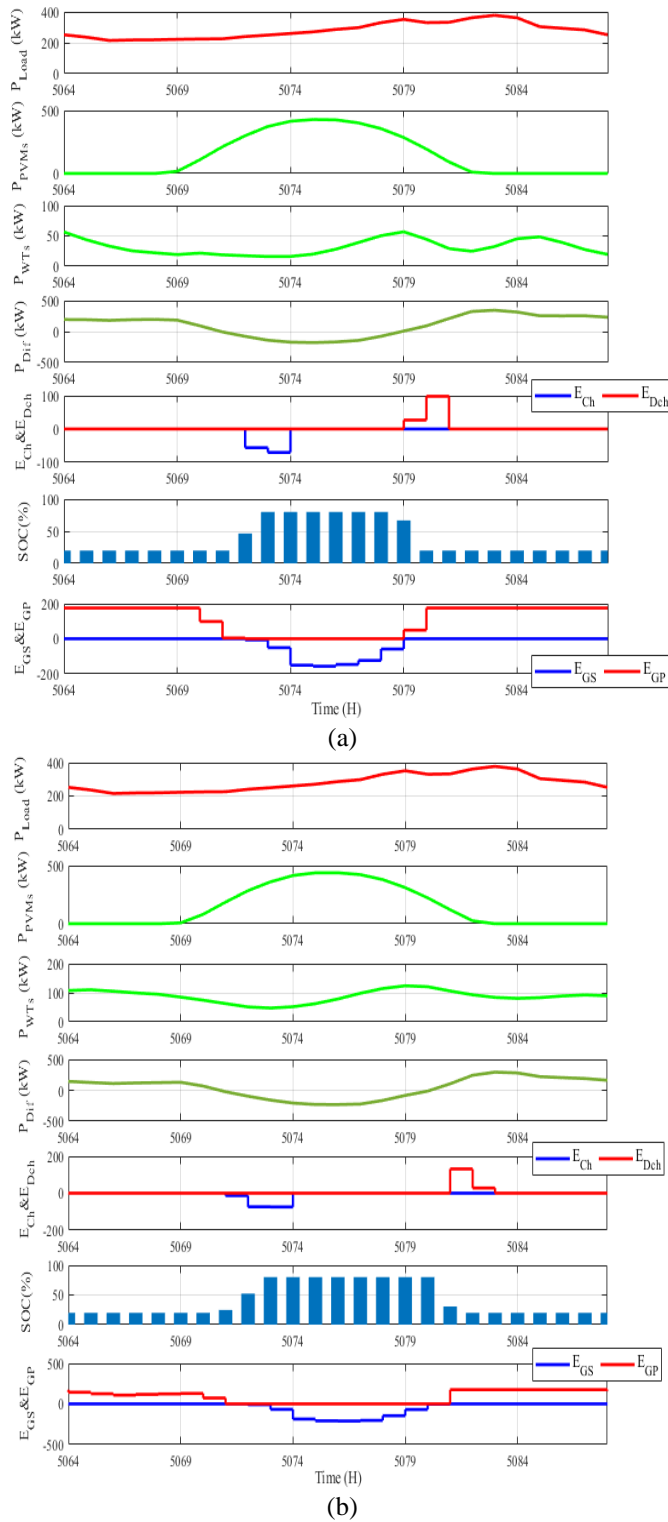


Fig. 10. ZOA technique results for a specific summertime day (24 h) of operation in a) Ras Sudr, and b) New Alamein city.

Taking into account the previously presented weather data, it is evident that New Alamein experiences higher wind speeds in comparison to Ras Sudr. To be more precise, New Alamein records an annual average wind speed of 5.97 m/s, whereas Ras Sudr reports an average wind speed of 5.82 m/s annually. A significant portion, specifically 79%, of the total energy required to meet the demand is sourced from available

sustainable sources (45% from WTs & 34% from PV). The remaining 21% is procured from the electric grid, as depicted in Fig. 11(b). In contrast, when considering the overall energy consumption, 77% is utilized to fulfill the load demand, and the remaining 23% is sold back to the utility grid.

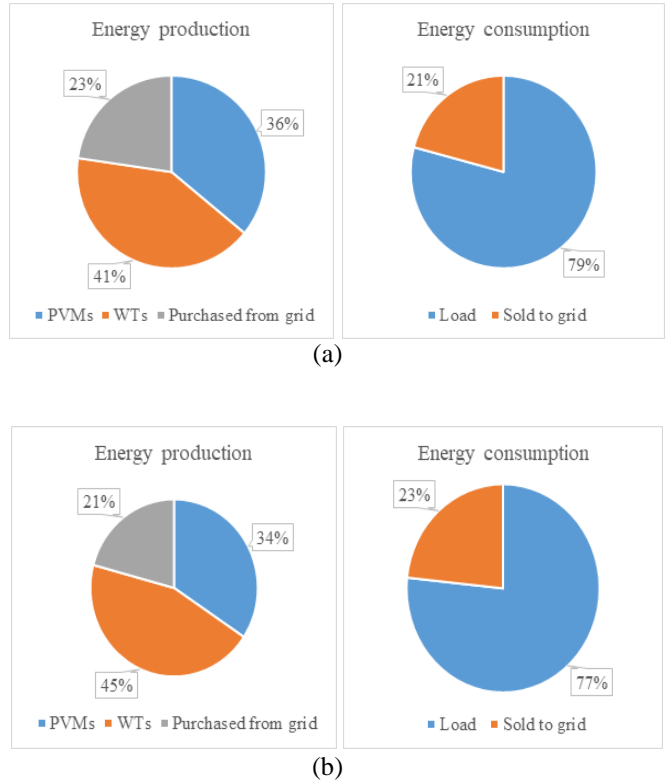


Fig. 11. Percentage of energy produced and consumed annually applying ZOA in a) Ras Sudr, and b) New Alamein city.

To ascertain the effectiveness and resilience of the ZOA optimizer, a total of 30 separate times to run were executed for each algorithm. Table 3 provides a statistical analysis of the results obtained from both optimizers, showcasing the best, worst, standard deviation, and mean values of the objective function. The results reveal that the ZOA optimizer exhibits a notably lower standard deviation in comparison to ASO, signifying the greater robustness of the ZOA algorithm. Figure 12 displays the convergence curves across 30 separate runs for both algorithms. Notably, ZOA identified the optimal solution on its 14th run, while ASO attained this on its 30th run, as illustrated in Fig. 13.

Table 3. Statistics of the results for ASO and ZOA

Statistics	Ras Sudr		New Alamein city	
	ASO	ZOA	ASO	ZOA
Best	0.0844	0.084257	0.079149	0.078943
Worst	0.0866	0.084263	0.082245	0.078957
Mean	0.0854	0.084258	0.080099	0.078944
Standard deviation	4.8089 * 10 ⁻⁴	1.8113 * 10 ⁻⁶	7.4679 * 10 ⁻⁴	2.7886 * 10 ⁻⁶
Rank	2	1	2	1

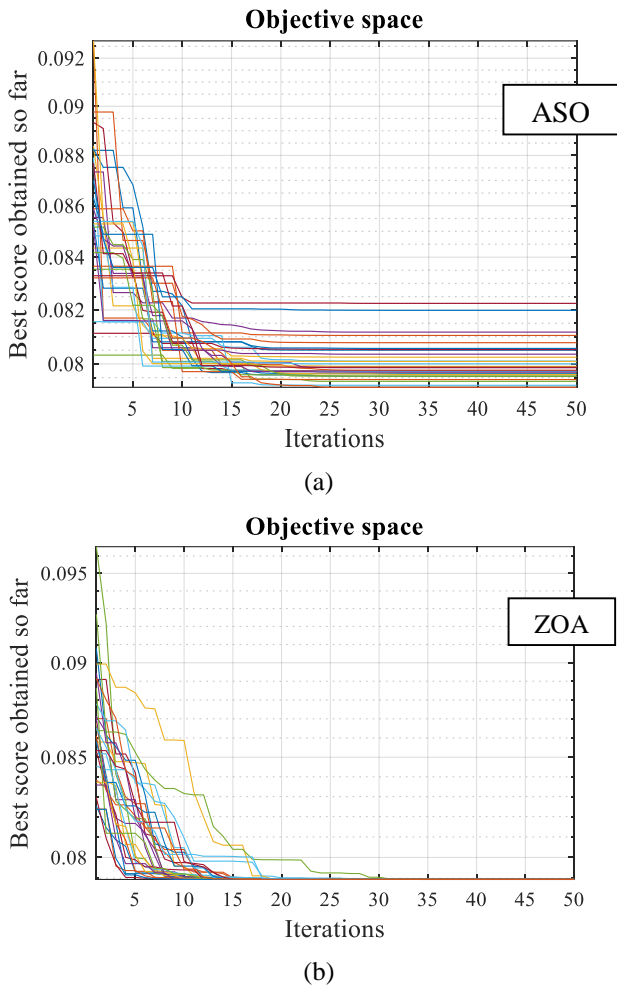


Fig. 12. Convergence performance of 30 separate times to run in New Alamein city case for a) ASO, and b) ZOA.

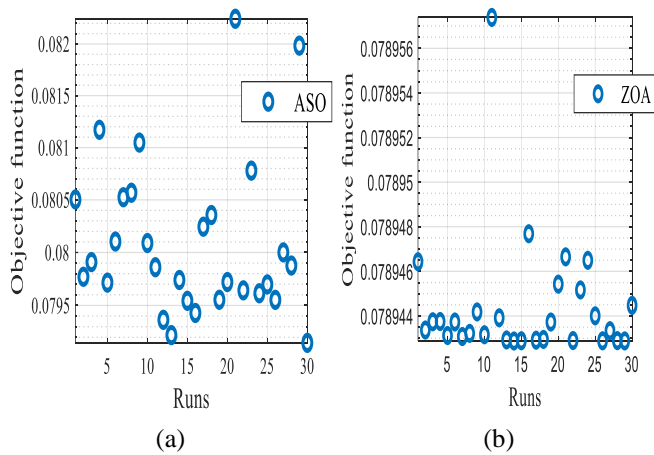


Fig. 13. Final results of 30 separate times to run in New Alamein city case with a) ASO, and b) ZOA.

5. Conclusion

This study has detailed the design and analysis of a grid-tied hybrid system integrating PV modules, WTs, and BBs for two various geographical areas in Egypt. To determine the optimal construction of the suggested grid-tied HRPS, two

optimizers have been utilized and examined using the MATLAB program. The overall sizing challenges are formulated to achieve equilibrium among three key objectives: minimizing COE, reducing LPSP, and curbing CO₂ emissions. Two scenarios are examined to assess the performance of utilized optimizers: the first case study took place in Ras Sudr, while the last one is conducted in New Alamein. Furthermore, a robustness test is employed through statistical analysis to assess and contrast the performance of the ASO and ZOA algorithms. The outcomes unequivocally demonstrated the superiority of the ZOA algorithm in achieving the optimal solution compared to ASO. Based on the results obtained for the Ras Sudr site, it is evident that the ZOA algorithm yields the lowest values for the following criteria: COE of 0.104073 \$/kWh, LPSP of 2.4967×10^{-10} , and CO₂ emissions of 426,273.75 kg/year. While in the case of New Alamein, ZOA managed to achieve the lowest values for the following indexes: COE of 0.096106 \$/kWh, LPSP of 1.5244×10^{-10} , and CO₂ emissions of 405,005.67 kg/year. The results clearly demonstrate that installing this hybrid system in the New Alamein region would result in savings of NPC amounting to 233,373 \$ and a reduction of annual carbon emissions by 21,268 kg. Future research works could incorporate additional renewable energy sources and diverse storage technologies. Moreover, while a grid-connected hybrid system with battery storage proves optimal in this study, hydrogen energy storage may present valuable prospects in various practical environments, warranting further investigation.

References

- [1] M. D. A. Al-Falahi, S. D. G. Jayasinghe, and H. Enshaei, “A review on recent size optimization methodologies for standalone solar and wind hybrid renewable energy system”, *Energy Conversion and Management*, vol. 143. Elsevier Ltd, pp. 252–274, 2017. doi: 10.1016/j.enconman.2017.04.019.
- [2] S. M. S. Hosseinimoghdam, H. Roghanian, M. Dashtdar, and S. M. Razavi, “Size optimization of distributed generation resources in microgrid based on scenario tree”, in *2020 8th International Conference on Smart Grid (icSmartGrid)*, 2020, pp. 67–72. doi: 10.1109/icSmartGrid49881.2020.9144968.
- [3] “International Energy Agency.” <https://www.iea.org/reports/world-energy-outlook-2021/executive-summary> (accessed Aug. 24, 2023).
- [4] M. H. Balali, N. Nouri, E. Omrani, A. Nasiri, and W. Otieno, “An overview of the environmental, economic, and material developments of the solar and wind sources coupled with the energy storage systems”, *Int. J. Energy Res.*, vol. 41, no. 14, pp. 1948–1962, 2017.
- [5] M. Nasser, T. F. Megahed, S. Ookawara, and H. Hassan, “Techno-economic assessment of clean hydrogen production and storage using hybrid renewable energy system of PV/wind under different climatic conditions”, *Sustain. Energy Technol. Assessments*, vol. 52, pp. 1–14, 2022, doi: 10.1016/j.seta.2022.102195.

- [6] M. M. Gamil, T. Senjyu, H. Takahashi, A. M. Hemeida, N. Krishna, and M. E. Lotfy, "Optimal multi-objective sizing of a residential microgrid in Egypt with different ToU demand response percentages", *Sustain. Cities Soc.*, vol. 75, pp. 1–16, 2021, doi: 10.1016/j.scs.2021.103293.
- [7] M. Stadler, G. Cardoso, S. Mashayekh, T. Forget, N. DeForest, A. Agarwal, and A. Schönbein, "Value streams in microgrids: A literature review", *Appl. Energy*, vol. 162, pp. 980–989, 2016, doi: 10.1016/j.apenergy.2015.10.081.
- [8] M. Abdelsattar, I. Hamdan, A. Mesalam, and A. Fawzi, "An overview of smart grid technology integration with hybrid energy systems based on demand response", in *2022 23rd International Middle East Power Systems Conference (MEPCON)*, IEEE, 2022, pp. 1–6.
- [9] H. Yang, W. Zhou, L. Lu, and Z. Fang, "Optimal sizing method for stand-alone hybrid solar-wind system with LPSP technology by using genetic algorithm", *Sol. Energy*, vol. 82, no. 4, pp. 354–367, 2008, doi: 10.1016/j.solener.2007.08.005.
- [10] S. Sanajaoba and E. Fernandez, "Maiden application of Cuckoo Search algorithm for optimal sizing of a remote hybrid renewable energy System", *Renew. Energy*, vol. 96, pp. 1–10, Oct. 2016, doi: 10.1016/j.renene.2016.04.069.
- [11] O. Ekren and B. Y. Ekren, "Size optimization of a PV/wind hybrid energy conversion system with battery storage using simulated annealing", *Appl. Energy*, vol. 87, no. 2, pp. 592–598, 2010, doi: 10.1016/j.apenergy.2009.05.022.
- [12] H. Sun, A. G. Ebadi, M. Toughani, S. A. Nowdeh, A. Naderipour, and A. Abdullah, "Designing framework of hybrid photovoltaic-biowaste energy system with hydrogen storage considering economic and technical indices using whale optimization algorithm", *Energy*, vol. 238, 2022, doi: <https://doi.org/10.1016/j.energy.2021.121555>.
- [13] D. K. Geleta, M. S. Manshahia, P. Vasant, and A. Banik, "Grey wolf optimizer for optimal sizing of hybrid wind and solar renewable energy system", *Comput. Intell.*, vol. 38, no. 3, pp. 1133–1162, 2022, doi: 10.1111/coin.12349.
- [14] W. Zhu, J. Guo, G. Zhao, and B. Zeng, "Optimal sizing of an island hybrid microgrid based on improved multi-objective grey wolf optimizer", *Processes*, vol. 8, no. 12, pp. 1–24, 2020, doi: 10.3390/pr8121581.
- [15] S. Mishra, G. Saini, A. Chauhan, S. Upadhyay, and D. Balakrishnan, "Optimal sizing and assessment of grid-tied hybrid renewable energy system for electrification of rural site", *Renew. Energy Focus*, vol. 44, pp. 259–276, 2023, doi: <https://doi.org/10.1016/j.ref.2022.12.009>.
- [16] F. S. Mahmoud, A. M. Abdelhamid, A. Al Sumaiti, A. H. M. El-Sayed, and A. A. Z. Diab, "Sizing and Design of a PV-Wind-Fuel Cell Storage System Integrated into a Grid Considering the Uncertainty of Load Demand Using the Marine Predators Algorithm", *Mathematics*, vol. 10, no. 19, 2022, doi: 10.3390/math10193708.
- [17] G. Lei, H. Song, and D. Rodriguez, "Power generation cost minimization of the grid-connected hybrid renewable energy system through optimal sizing using the modified seagull optimization technique", *Energy Reports*, vol. 6, pp. 3365–3376, 2020.
- [18] S. Barakat, M. M. Samy, M. B. Eteiba, and W. I. Wahba, "Viability study of grid connected PV/Wind/Biomass hybrid energy system for a small village in Egypt", *2016 18th Int. Middle-East Power Syst. Conf. MEPCON 2016 - Proc.*, pp. 46–51, 2017, doi: 10.1109/MEPCON.2016.7836870.
- [19] A. A. Z. Diab, H. M. Sultan, and O. N. Kuznetsov, "Optimal sizing of hybrid solar/wind/hydroelectric pumped storage energy system in Egypt based on different meta-heuristic techniques", doi: 10.1007/s11356-019-06566-0/Published.
- [20] V. K. Garg and S. Sharma, "Optimum sizing and economic assessment of hybrid microgrid for domestic load under various scenario", *Int. J. Renew. Energy Res.*, vol. 11, no. 1, pp. 235–246, 2021, doi: 10.20508/ijrer.v11i1.11760.g8128.
- [21] S. S. Yusuf and N. N. Mustafi, "Design and simulation of an optimal mini-grid solar-diesel hybrid power generation system in a remote Bangladesh", *Int. J. Smart grid*, vol. 2, no. 1, 2018, doi: 10.20508/ijsmartgrid.v2i1.7.g8.
- [22] G. Gursoy and M. Baysal, "Improved optimal sizing of hybrid PV/wind/battery energy systems", *3rd Int. Conf. Renew. Energy Res. Appl. ICRERA 2014*, no. 2, pp. 713–716, 2014, doi: 10.1109/ICRERA.2014.7016478.
- [23] F. S. Mahmoud, A. A. Zaki Diab, Z. M. Ali, A. M. El-Sayed, T. Alquthami, M. Ahmed, and H. A. Ramadan, "Optimal sizing of smart hybrid renewable energy system using different optimization algorithms", *Energy Reports*, vol. 8, pp. 4935–4956, 2022, doi: 10.1016/j.egy.2022.03.197.
- [24] F. M. Wulfran, D. Naoussi, S. Raoul, M. Reagan, and J. Jacques, "A technical analysis of a grid-connected hybrid renewable energy system under meteorological constraints for a timely energy management", *Int. J. Smart grid*, vol. 7, no. V7i2, 2023, doi: 10.20508/ijsmartgrid.v7i2.278.g260.
- [25] A. F. Güven, N. Yörükeren, and M. M. Samy, "Design optimization of a stand-alone green energy system of university campus based on Jaya-Harmony Search and Ant Colony Optimization algorithms approaches",

- Energy, vol. 253, Aug. 2022, doi: 10.1016/j.energy.2022.124089.
- [26] J. Zhou and Z. Xu, "Optimal sizing design and integrated cost-benefit assessment of stand-alone microgrid system with different energy storage employing chameleon swarm algorithm: A rural case in Northeast China", *Renew. Energy*, vol. 202, pp. 1110–1137, Jan. 2023, doi: 10.1016/j.renene.2022.12.005.
- [27] R. Khezri, A. Mahmoudi, and M. H. Haque, "Optimal capacity of solar PV and battery storage for Australian grid-connected households", *IEEE Trans. Ind. Appl.*, vol. 56, no. 5, pp. 5319–5329, 2020, doi: 10.1109/TIA.2020.2998668.
- [28] A. S. Al-Buraiki and A. Al-Sharafi, "Hydrogen production via using excess electric energy of an off-grid hybrid solar/wind system based on a novel performance indicator", *Energy Convers. Manag.*, vol. 254, Feb. 2022, doi: 10.1016/j.enconman.2022.115270.
- [29] S. Singh, P. Chauhan, and N. J. Singh, "Capacity optimization of grid connected solar/fuel cell energy system using hybrid ABC-PSO algorithm", *Int. J. Hydrogen Energy*, vol. 45, no. 16, pp. 10070–10088, 2020, doi: 10.1016/j.ijhydene.2020.02.018.
- [30] A. A. Zaki Diab, S. I. El-Ajmi, H. M. Sultan, and Y. B. Hassan, "Modified farmland fertility optimization algorithm for optimal design of a grid-connected hybrid renewable energy system with fuel cell storage: Case study of Ataka, Egypt", *Int. J. Adv. Comput. Sci. Appl.*, vol. 10, no. 8, pp. 119–132, 2019.
- [31] M. Nurunnabi, N. K. Roy, and H. R. Pota, "Optimal sizing of grid-tied hybrid renewable energy systems considering inverter to PV ratio - A case study", *J. Renew. Sustain. Energy*, vol. 11, no. 1, 2019, doi: 10.1063/1.5052492.
- [32] I. M. Opedare, T. M. Adekoya, and A. E. Longe, "Optimal sizing of hybrid renewable energy system for off-grid electrification: a case study of university of Ibadan Abdusalam Abubakar Post Graduate Hall of Residence", *Int. J. Smart grid*, vol. 4, no. 4, 2020, doi: 10.20508/ijsmartgrid.v4i4.135.g110.
- [33] A. M. Eltamaly, M. A. Mohamed, and A. I. Alolah, "A novel smart grid theory for optimal sizing of hybrid renewable energy systems", *Sol. Energy*, vol. 124, pp. 26–38, Feb. 2016, doi: 10.1016/j.solener.2015.11.016.
- [34] H. N. Afrouzi, A. Hassan, Y. P. Wimalaratna, J. Ahmed, K. Mehrazamir, S. C. Liew, and Z. Abdul Malek, "Sizing and economic analysis of stand-alone hybrid photovoltaic-wind system for rural electrification: A case study Lundu, Sarawak", *Clean. Eng. Technol.*, vol. 4, Oct. 2021, doi: 10.1016/j.clet.2021.100191.
- [35] A. Maleki and F. Pourfayaz, "Optimal sizing of autonomous hybrid photovoltaic/wind/battery power system with LPSP technology by using evolutionary algorithms", *Sol. Energy*, vol. 115, pp. 471–483, 2015, doi: 10.1016/j.solener.2015.03.004.
- [36] S. A. Mohamed and M. Abd El Sattar, "A comparative study of P&O and INC maximum power point tracking techniques for grid-connected PV systems", *SN Appl. Sci.*, vol. 1, no. 2, pp. 1–13, 2019, doi: 10.1007/s42452-018-0134-4.
- [37] S. Singh and S. C. Kaushik, "Optimal sizing of grid integrated hybrid PV-biomass energy system using artificial bee colony algorithm", *IET Renew. Power Gener.*, vol. 10, no. 5, pp. 642–650, 2016, doi: 10.1049/iet-rpg.2015.0298.
- [38] E. E. E. Ahmed, A. Demirci, and S. M. Tercan, "Optimal sizing and techno-enviro-economic feasibility assessment of solar tracker-based hybrid energy systems for rural electrification in Sudan", *Renew. Energy*, vol. 205, pp. 1057–1070, Mar. 2023, doi: 10.1016/j.renene.2023.02.022.
- [39] O. Nadjemi, T. Nacer, A. Hamidat, and H. Salhi, "Optimal hybrid PV/wind energy system sizing: Application of cuckoo search algorithm for Algerian dairy farms", *Renew. Sustain. Energy Rev.*, vol. 70, no. November 2015, pp. 1352–1365, 2017, doi: 10.1016/j.rser.2016.12.038.
- [40] S. Barakat, M. M. Samy, M. B. Eteiba, and W. I. Wahba, "Feasibility study of grid connected pv-biomass integrated energy system in Egypt", *Int. J. Emerg. Electr. Power Syst.*, vol. 17, no. 5, pp. 519–528, 2016, doi: 10.1515/ijeeps-2016-0056.
- [41] E. Trojovska, M. Dehghani, and P. Trojovsky, "Zebra optimization algorithm: a new bio-inspired optimization algorithm for solving optimization algorithm", *IEEE Access*, vol. 10, pp. 49445–49473, 2022, doi: 10.1109/ACCESS.2022.3172789.
- [42] W. Zhao, L. Wang, and Z. Zhang, "A novel atom search optimization for dispersion coefficient estimation in groundwater", *Futur. Gener. Comput. Syst.*, vol. 91, pp. 601–610, 2019, doi: 10.1016/j.future.2018.05.037.
- [43] W. Zhao, L. Wang, and Z. Zhang, "Atom search optimization and its application to solve a hydrogeologic parameter estimation problem", *Knowledge-Based Syst.*, vol. 163, pp. 283–304, 2019, doi: 10.1016/j.knosys.2018.08.030.
- [44] "NASA POWER." <https://power.larc.nasa.gov/data-access-viewer/> (accessed Aug. 22, 2023).
- [45] A. A. Zaki Diab, H. M. Sultan, I. S. Mohamed, N. Kuznetsov Oleg, and T. D. Do, "Application of different optimization algorithms for optimal sizing of PV/wind/diesel/battery storage stand-alone hybrid microgrid", *IEEE Access*, vol. 7, pp. 119223–119245, 2019, doi: 10.1109/ACCESS.2019.2936656.